Materials Advances

ROYAL SOCIETY OF CHEMISTRY

PAPER

View Article Online
View Journal | View Issue

Cite this: *Mater. Adv.*, 2025, **6**, 1965

Tri(oxyethylene)-functionalised perylene diimide: a promising interlayer material for enhanced organic photovoltaic performance†

Jegadesan Subbiah, *[a] Akhil Gupta, [b] David J. Jones *[a] and Jingliang Li *[b]

Received 13th January 2025,
Accepted 11th February 2025

DOI: 10.1039/d5ma00032g

rsc.li/materials-advances

Interface engineering of organic semiconductors is critical for efficient charge extraction from organic photoactive layers to inorganic electrodes, which is a key factor in optimising organic solar cell performance. Incorporating polar groups into electron transport layer (ETL) materials can reduce their work function by forming appropriate dipoles between the photoactive layer and the electrode. This study reports a promising ETL material, 2,9-bis(2-(2-(2-methoxyethoxy)ethoxy)ethyl)anthra[2,1,9-*def*:6,5,10-*d′e′f′*]diisoquinoline-1,3,8,10(2*H*,9*H*)-tetraone, coded **PDIAO**, based on a perylene diimide (PDI) core with tri(oxyethylene) chains at the imide positions. **PDIAO** exhibited efficient energy level alignment and good interface contact with the active layer, facilitating efficient electron extraction. Organic photovoltaic (OPV) devices with the **PM6:IT-4F** active layer, a **PDIAO** interlayer, demonstrated enhanced performance, achieving a power conversion efficiency (PCE) of 13% compared to the PCE of 10.9% for the OPV device with the **PFN-Br** interlayer. Various spectroscopic and electrical characterisation analyses of ETL materials and OPV device performance revealed that the **PDIAO** interlayer significantly reduces the work function of the active layer by forming interface dipole and enhanced charge transport for efficient electron extraction. These results suggest that tri(oxyethylene)-functionalised PDI derivatives are promising ETL materials for efficient electron extraction in OPV devices.

Introduction

The increasing demand for energy and growing awareness of environmental and pollution problems have made developing clean and renewable energy technologies a pressing research priority.[1] Organic solar cells, with their unique properties of flexibility, semi-transparency, low cost, large-area applicability, and lightweight design, have emerged as a promising alternative to traditional energy sources.[2–5] Recent advancements in the molecular structure of polymer donors, fused ring electron acceptors, and optimisation of bulk heterojunction morphology and device geometry have significantly boosted the power conversion efficiency (PCE) of single-junction organic photovoltaic (OPV) devices, exceeding 20%.[6–8] Interface engineering, particularly the development of new interlayer materials, is crucial for further enhancing the performance of OPV devices and realising their practical applications.[9–11] Despite significant progress in OPV research, limited studies have focused on the design and development of molecular interlayer materials, especially for non-fullerene acceptor (NFA)-based organic solar cells.[12–17] Our research has focused on developing promising, high-performance interlayer materials for organic solar cells, particularly (oxyethylene)-functionalised PDI derivatives. We are now exploring tri(oxyethylene)-functionalised PDI derivatives as promising interlayer materials for future high-performance OPV devices. We believe that these materials have the potential to significantly improve the performance of OPV devices by enhancing charge extraction and interfacial properties.

Interlayer materials play a crucial role in providing Ohmic contact between the organic active layer and metal electrode, thereby reducing the energy barrier and facilitating charge transport.[18,19] In OPV devices, most interlayers are based on inorganic layers such as TiO_2, ZnO, SnO_2, *etc.*[20,21] These materials require high-temperature treatment for efficient performance, limiting their use in flexible substrates. Polymer-based ETL layers such as PFN, PEIE, and **PFN-Br** are widely used in OPV devices for efficient electron extraction.[22,23] However, the variability of these polymer materials in batch-to-batch and molecular weight control can hinder their use in OPV device fabrication. This highlights the urgent need for research and

[a] *School of Chemistry, Bio21 Institute, The University of Melbourne, Parkville, VIC 3010, Australia. E-mail: jsubbiah@unimelb.edu.au, djjones@unimelb.edu.au*
[b] *Institute for Frontier Materials, Deakin University, Geelong, VIC 3216, Australia. E-mail: jingliang.li@deakin.edu.au*

† Electronic supplementary information (ESI) available: Synthetic details, spectroscopic, optical and electrochemical characterisation, and OPV and conductivity device diagrams. See DOI: https://doi.org/10.1039/d5ma00032g

development in this area. Small molecule-based ETL materials such as **PDIN**, **PDINO**, PDINN, and PFN-2TNDI offer advantages over polymer-based materials.[12,24,25] They exhibit good repeatability in synthesis, ensuring high purity and leading to superior device performance in non-fullerene-based OPV devices. These materials can form interfacial dipoles, providing ohmic contact and facilitating efficient electron extraction.[12,24–26]

As mentioned above, and given that PDI-based materials offer excellent electron transport properties, we prepared a tri(oxyethylene)-functionalised PDI derivative by directly attaching tri(ethylene glycol) methyl ether amine units to the perylene unit at the imide positions to generate PDIAO. This was done to provide good Ohmic contact for efficient electron transport.[27,28] It is notable that this target material has been reported previously in the literature, where it was studied for its selectivity toward G-rich DNA capable of forming quadruplex structures[29] and used as an efficient electron shuttle for reactions with O_2.[30] Our motivation for using such amine units is based on the proven fact that these units can help improve surface morphology and, consequently, the overall performance of OPV devices.[31] The multiple oxygen groups in the tri(oxyethylene) chain enhance the dipole moment, improving the ability to modify the work function for an effective electron interface layer.[28,32] To compare the performance of PDI with tri(oxyethylene) side chain ETL materials, we also synthesised the ETL materials with aliphatic group- and aliphatic amine group-functionalised PDI molecules. All three materials were synthesised and used as ETL materials in OPV devices to evaluate their performance. Using the tri(oxyethylene) sidechain-based ETL materials as a cathode interlayer, the device with **PM6:IT-4F** active layer exhibited enhanced performance with an average PCE of 13%. These results suggest that the polar-rich side chain functionalised PDI materials are a good candidate for ETL materials for future large-area applications of OPV devices.

Results and discussion

Fig. 1a shows the molecular structures of PDI-based small-molecules and the device geometry used to fabricate OPV devices. Detailed synthetic routes and characterisation data for the studied ETL materials are given in the ESI.† The purity and structures of the reported molecules were confirmed using NMR (^{1}H and ^{13}C) and mass spectroscopy; the details are shown in Fig. S1 (ESI†). It should be noted that the synthetic route we used to generate **PDIAO**, in particular, differs from that previously reported.[29] We conducted a direct reaction between 3,4,9,10-perylenetetracarboxylic dianhydride and 2-(2-(2-methoxyethoxy)ethoxy) ethanamine using dry ethanol, refluxing the reaction mixture overnight. The target material was directly filtered as a dark red powder. Our synthetic strategy presents no synthetic challenges and can generate larger quantities if required for device optimization and further study. The synthesised PDI derivatives are soluble in chloroform, chlorobenzene, toluene, trifluoroethanol, and trifluorotoluene and sparingly soluble in methanol solvents. The absorption spectroscopy of **PDIN**, PDINA and PDINAO in chloroform solution and pristine

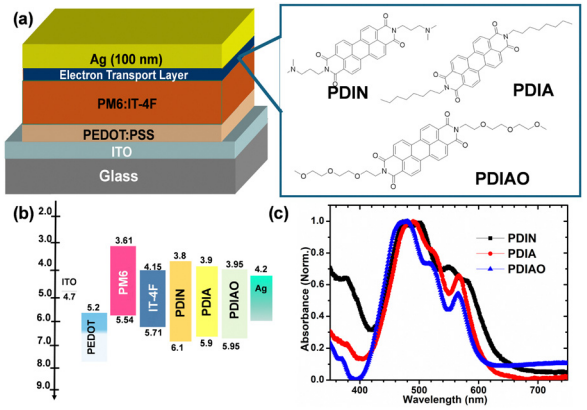

Fig. 1 (a) Schematic diagram of the investigated OPV devices and molecular structures of ETL materials, (b) energy levels of various materials used in OPV devices and (c) optical absorption spectra of solid state ETL materials.

thin films are given in Fig. S2 (ESI†) and Fig. 1c, respectively. Table 1 summarises the maximum absorption peak and onset absorption details for solution and solid states of ETL materials, **PDIN**, PDINA and PDINAO. Using the onset absorption of thin film UV-vis absorption spectra, the optical band gaps of **PDIN**, **PDIA** and **PDIAO** were calculated as 1.94 eV, 2.00 eV and 2.06 eV, respectively.

Compared to the **PDIN** film, the **PDIAO** film exhibits blue-shifted absorption with an absorption edge of 600 nm, suggesting strong aggregation properties due to the polar oxygen functionalised sidechain. This observation is consistent with previous reports on the influence of polar side chains on the aggregation behavior of PDI-based materials[33] To determine the highest occupied molecular orbital (HOMO) and the lowest unoccupied molecular orbital (LUMO) energy levels of ETL materials, cyclic voltammetry measurements were carried out. The energy level values are given in Table 1. Fig. S3 (ESI†) showed the onset oxidation (ϕ_{ox}) and reduction potentials (ϕ_{red}) of ETL materials. The energy levels (HOMO and LUMO) of all the materials were calculated using the equation $E_{HOMO/LUMO} = -e(\phi_{ox/red} - \phi_{Fc^+/Fc} + 4.8)$ eV. The HOMO energy values of **PDIN**, **PDIA** and **PDIAO** are calculated as 6.10 eV, 5.90 eV and 5.95 eV, respectively. The deep HOMO values effectively block the holes at the cathode. The LUMO values of **PDIN**, **PDIA**, and **PDIAO** were calculated as 3.80 eV, 3.90 eV, and 3.95 eV, respectively. Notably, the LUMO value of **PDIAO** is very close to the acceptor LUMO level, and it provides improved energy level alignment at the cathode interface and facilitates efficient electron extraction.

Table 1 Optical and electrochemical characterisation of ETL materials

ETL	Optical absorption (λ_{max}, λ_{onset}) (nm)		Band gap (E_g) eV	Cyclic voltammetry (eV)		
	Solution	Film		HOMO	LUMO	E_g
PDIN	530 547	500 640	1.94	−6.10	−3.80	2.3
PDIA	525 542	580 620	2.00	−5.90	−3.90	2.0
PDIAO	525 542	570 600	2.06	−5.95	−3.95	2.0

To investigate the effect of ETL materials on electron collection efficiency, we have fabricated OPV devices with the conventional device geometry, ITO/PEDOT:PSS/**PM6:IT-4F**/ETL/Ag, as is shown in Fig. 1a. The energy levels of all the materials used in device fabrication are shown in Fig. 1b, and the molecular structures of polymer **PM6**, NFAs **IT-4F** and **Y6** are shown in Fig. 2a. The *J*–*V* curves of the OPV devices with the ETL of **PFN-Br**, **PDIN**, **PDIA** and **PDIAO** are shown in Fig. 2b, and the corresponding device characteristics parameters are given in Table 2. Here, the control device with a **PFN-Br** interlayer shows a PCE of 12.1% (with a J_{sc} of 20.3 mA cm^{-2}, V_{oc} of 0.80 V and fill factor (FF) of 73%), whereas the device with a **PDIN** interlayer exhibits a PCE of 12.25% (with J_{sc} of 20.7 mA cm^{-2}, V_{oc} of 0.82 V and FF of 74%). These results indicate that the **PDIN** interlayer has a significant advantage over the **PFN-Br** interlayer in improving the device performance of NFA-based OPV devices. The OPV device with the **PDIA** interlayer shows lower performance with a PCE of 9.9%, which might be attributed to a lack of functional groups in the sidechain groups. The device with a 10 nm **PDIAO** layer delivers superior performance with the best PCE of 13.3% (average PCE of 13%), compared to the device with other ETLs such as **PFN-Br**, **PDIN** and **PDIA**. The enhanced performance is primarily due to increased FF, J_{sc} and V_{oc} values. Here, the maximum thickness for the spin-coated ETL layer is 10 nm; further increase in ETL thickness reduces the device performance.

The external quantum efficiency plot (Fig. 2c) of OPV devices with **PDIN**, **PDIA** and **PDIAO** interlayers confirms the reliability of measured J_{sc} values. The integrated J_{sc} values, which are calculated from EQE plot of the OPV devices based on **PFN-Br**, **PDIN**, **PDIA** and **PDIAO** ETL layers, are 18.9, 19.2, 18.0 and 20.1 mA cm^{-2}, respectively, which are in good agreement with the measured J_{sc} values within 5% error. To further evaluate the performance of **PDIAO** interlayer, we investigated its use in OPV devices with **PM6:Y6** active layers. The device performances are given in Fig. S4 (ESI†). As summarised in Table S1 (ESI†), the OPV device with a **PM6:Y6** active layer and **PDIAO** interlayer exhibits the best performance of 16.1%, compared to the 15.2% PCE of the device with the **PFN-Br** interlayer. These results suggest that the **PDIAO** ETL layer is a promising candidate for use in various NFA-based OPV devices as an efficient cathode interlayer.

To explore the effect of ETL layers on the device performance, we studied the electronic properties, such as work function and the HOMO energy level, to understand the energy level alignment of the photoactive layer with various ETL layer materials using ultraviolet photoelectron spectroscopy (UPS).[12] The secondary electron cut-off edge of the UPS spectrum provides the work function of the materials, as shown in Fig. 3a. The electronic parameter characteristics are given in Table 3. Fig. 3a demonstrates that the work function of the **PM6:IT-4F** blend film is 4.52 eV. When coating the ETL layer on top of the active layer, the work function value decreases to 4.27, 4.37 and 4.17 eV for the **PDIN**, **PDIA** and **PDIAO** based layers, respectively. Here, **PDIAO** exhibited a more substantial work function reduction ability compared to other ETL layers, suggesting the formation of an appropriate interface dipole between the active layer and metal contact to provide Ohmic contact. This reduced energy barrier facilitates efficient charge extraction, leading to improved J_{sc}, V_{oc} and FF in OPV devices.

The HOMO level of the active layer film with and without ETL layers was calculated from the low-binding energy edge of

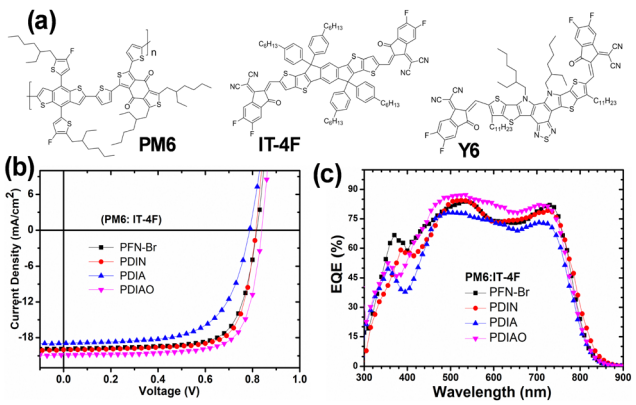

Fig. 2 (a) Molecular structures of the donor polymer **PM6** and non-fullerene acceptors **IT-4F** and **Y6**, (b) *J*–*V* plot and (c) EQE of the OPV devices with various cathode interlayers.

Table 2 Photovoltaic characteristics of the OPV devices with various cathode interlayer materials

ETL	J_{sc} (mA cm^{-2})	V_{oc} (V)	FF (%)	PCE (%)[a] (best cell)
PFN-Br	20.3 ± 0.25	0.80 ± 0.02	73 ± 2	11.8 ± 0.25 (12.10)
PDIN	20.7 ± 0.20	0.82 ± 0.02	74 ± 3	11.9 ± 0.30 (12.25)
PDIA	18.9 ± 0.30	0.76 ± 0.03	65 ± 3	9.8 ± 0.35 (9.90)
PDIAO	20.9 ± 0.25	0.84 ± 0.02	76 ± 2	13.0 ± 0.25 (13.30)

[a] PCE values are calculated using 12 devices for each active layer.

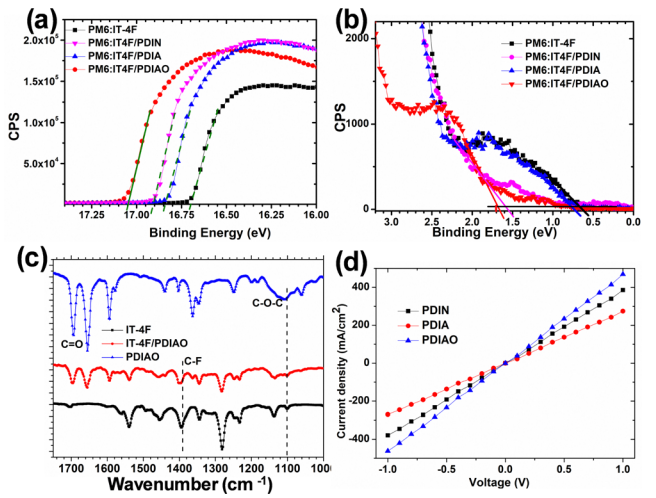

Fig. 3 (a) UPS spectra of secondary electron cut-off and (b) HOMO onset energy level of **PM6:IT-4F** blend layer with and without ETL materials, (c) FTIR spectra of **PDIAO** and **IT-4F** pristine and blend film, and (d) *I*–*V* plot of conductivity studies of ETL materials.

Table 3 UPS spectroscopy data of **PM6:IT-4F** blend film with and without various cathode interlayer materials

PM6:IT-4F/ETL	Secondary electron cut-off (eV)	Fermi level (eV)	Valence band edge (eV)	HOMO level (eV)
Without ETL	16.70	−4.52	0.6	−5.12
PDIN	16.85	−4.27	1.6	−5.87
PDIA	16.90	−4.37	0.7	−5.07
PDIAO	17.05	−4.17	1.7	−5.87

the UPS spectrum using the formula, $E_{HOMO} = h\nu - (E_{cutoff} - E_{onset})$, where $h\nu$ is the incident He I photon energy (21.22 eV), E_{cutoff} is the secondary electron cut-off energy and E_{onset} is HOMO level onset energy. As shown in Table 3, the HOMO level of the **PDIAO** layer is 5.87 eV, which is deeper than that of other ETL layers. The higher HOMO value provides efficient hole-blocking ability at the cathode interface. These UPS studies support the favourable energy level alignment of ETL layers for efficient ohmic contact with a reduced energy barrier at the cathode interface.

To investigate the effect of ETL layers on device performance, we studied the surface morphology of **PM6:IT-4F** blend films with and without the ETL layers using tapping mode AFM.[34] Fig. 4a shows the height and phase images of **PM6:IT-4F** blend film, revealing a nanoscale phase-separated morphology with a surface roughness of 1.46 nm. Upon coating the ETL layer on top of the active layer film, the phase-separated morphology was retained, but the surface roughness increased to 1.65, 1.76 and 2.1 nm for **PDIN**, **PDIA** and **PDIAO** interlayers, respectively. As shown in Fig. 4d, the **PDIAO** interlayer exhibited increased aggregation, confirming its interaction with the active layer. The polar groups of **PDIAO** likely interact with the active layer, causing aggregation and enhancing interface energetics, which can contribute to efficient charge extraction.[32]

To further confirm this interaction, we investigated the pristine film **IT-4F** film, **PDIAO**, and blend film of **IT-4F** and **PDIAO** using Fourier transform infrared spectroscopy. Fig. 3c shows that the broad C–O–C vibration band of the **PDIAO** ETL layer at 1100 cm^{-1} is suppressed in the blend film, indicating an interaction between the polar groups of **PDIAO** and the **IT-4F** acceptor. Additionally, the C–F vibration peak at 1390 cm^{-1} for **IT-4F** shifted to 1396 cm^{-1} in the **IT-4F** and **PDIAO** blend film, suggesting an interaction between the ETL layer and the active layer, leading to aggregation and favourable energy level alignment at the cathode interface.[32]

To evaluate the conductivity of the ETL layer, the *I–V* characteristics were measured by constructing a device composed of ITO/ETL film (10 nm)/Ag (100 nm), as shown in Fig. S5 (ESI†).[35] The conductivity of ETL materials was determined from the slope of the *J–V* plot (Fig. 3d) using the equation $\sigma = (Id/VA)$, where A is the area and d is the thickness of the ETL film. The conductivities of ETL layers, **PDIN**, **PDIA**, and **PDIAO**, were calculated as 3.82, 2.72, and 4.65 ($\times 10^{-6}$ S cm^{-1}), respectively. The conductivity of the **PDIAO** ETL layer is higher than that of the **PDIN** layer, which contributes to enhanced charge extraction and higher fill factor, leading to improved device performance. We also investigated the stability of OPV devices with **PFN-Br** and **PDIAO** interlayer without encapsulation and stored them in a glove box between *J–V* measurements. As shown in the ESI,† Fig. S6, the T80 lifetime was observed as 240 h for a control device with **PFN-Br** ETL, whereas the device based on the **PDIAO** layer shows 220 hours. These stability studies indicate that the **PDIAO** interlayer device possesses slightly lower stability performance than the state-of-the-art device with the **PFN-Br** interlayer device.[36]

Conclusions

To summarise, we developed a tri(oxyethylene)-functionalised PDI derivative, namely **PDIAO**, as a promising ETL material for

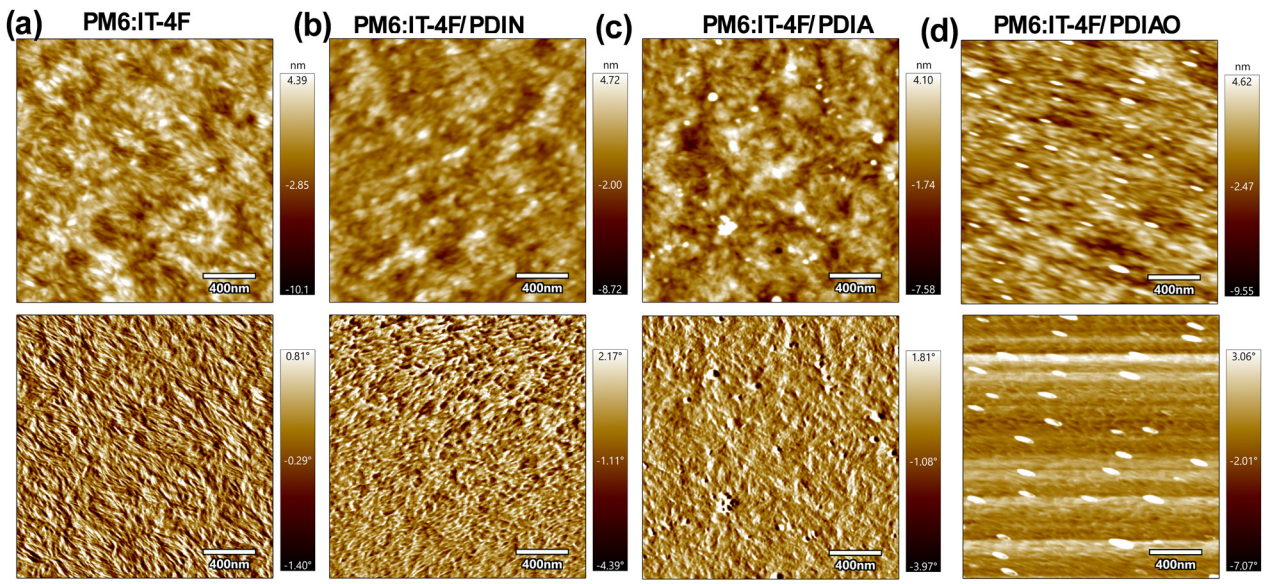

Fig. 4 AFM height (top) and phase (bottom) images of (a) **PM6:IT-4F** blend film, (b) **PM6:IT-4F/PDIN**, (c) **PM6:IT-4F/PDIA,** and (d) **PM6:IT-4F/PDIAO** film surfaces.

organic photovoltaic devices. Compared to other PDI derivatives, *i.e.*, **PDIN** and **PDIA**, the **PDIAO** interlayer consistently demonstrated superior charge extraction properties, leading to enhanced performance in both **PM6:IT-4F** and **PM6:Y6**-based OPV devices. The device with the **PM6:IT-4F** active layer and a **PDIAO** ETL delivers superior performance with the best PCE of 13.3%, compared to the device with other ETLs such as **PFN-Br** (12.10%), **PDIN** (12.25%), and **PDIA** (9.90%). In addition, the best efficiency of 16.1% was achieved with a **PM6:Y6** active layer and **PDIAO** interlayer. Characterisation studies, including UPS and FTIR analysis, revealed favorable energy level alignment, reduced interfacial barriers, and effective interactions between the **PDIAO** ETL layer and the active layer, contributing to efficient charge transport and improved device performance. These findings highlight the potential of tri(oxyethylene)-functionalised PDI derivatives as high-performance ETL materials for future advancements in OPV technology.

Data availability

The data supporting this article have been included as part of the ESI.†

Conflicts of interest

There are no conflicts to declare.

Acknowledgements

J. S. and J. L. acknowledge funding support from the Australian Government through the Australian Research Council's Discovery Projects funding scheme (DP 210100482). J. S. and D. J. J. are funded by the Australian Government through the Australian Centre for Advanced Photovoltaics (ACAP), the Australian Renewable Energy Agency (ARENA). The Australian Government does not accept responsibility for the views, information or advice expressed herein. This work was partly performed at the Materials Characterisation and Fabrication Platform (MCFP) at the University of Melbourne. The authors acknowledge the facilities and the technical assistance of the RMIT University Microscopy and Microanalysis Facility (RMMF).

References

1 J. Subbiah and D. J. Jones, in *Encyclopedia of Renewable Energy, Sustainability and the Environment*, ed. M. R. Rahimpour, Elsevier, Oxford, 4th edn, 2024, pp. 349–374, DOI: 10.1016/B978-0-323-93940-9.00147-X.
2 Y.-J. Heo, J.-E. Kim, H. Weerasinghe, D. Angmo, T. Qin, K. Sears, K. Hwang, Y.-S. Jung, J. Subbiah, D. J. Jones, M. Gao, D.-Y. Kim and D. Vak, *Nano Energy*, 2017, **41**, 443–451.
3 H. Yin, J. Yan, J. K. W. Ho, D. Liu, P. Bi, C. H. Y. Ho, X. Hao, J. Hou, G. Li and S. K. So, *Nano Energy*, 2019, **64**, 103950.
4 C. M. Amb, S. Chen, K. R. Graham, J. Subbiah, C. E. Small, F. So and J. R. Reynolds, *J. Am. Chem. Soc.*, 2011, **133**, 10062–10065.
5 V. K. Wong, C. Zhang, Z. Zhang, M. Hao, Y. Zhou and S. K. So, *Mater. Today Energy*, 2023, **36**, 101347.
6 S. Guan, Y. Li, C. Xu, N. Yin, C. Xu, C. Wang, M. Wang, Y. Xu, Q. Chen, D. Wang, L. Zuo and H. Chen, *Adv. Mater.*, 2024, **36**, 2400342.
7 C. Yan, S. Barlow, Z. Wang, H. Yan, A. K. Y. Jen, S. R. Marder and X. Zhan, *Nat. Rev. Mater.*, 2018, **3**, 18003.
8 J. Yuan, Y. Zhang, L. Zhou, G. Zhang, H.-L. Yip, T.-K. Lau, X. Lu, C. Zhu, H. Peng, P. A. Johnson, M. Leclerc, Y. Cao, J. Ulanski, Y. Li and Y. Zou, *Joule*, 2019, **3**, 1140–1151.
9 J. Subbiah, C. M. Amb, I. Irfan, Y. Gao, J. R. Reynolds and F. So, *ACS Appl. Mater. Interfaces*, 2012, **4**, 866–870.
10 M. J. Hartel, J. Subbiah and F. So, *J. Disp. Technol.*, 2013, **9**, 469–475.
11 C. Sun, Z. Wu, Z. Hu, J. Xiao, W. Zhao, H.-W. Li, Q.-Y. Li, S.-W. Tsang, Y.-X. Xu, K. Zhang, H.-L. Yip, J. Hou, F. Huang and Y. Cao, *Energy Environ. Sci.*, 2017, **10**, 1784–1791.
12 J. Yao, B. Qiu, Z.-G. Zhang, L. Xue, R. Wang, C. Zhang, S. Chen, Q. Zhou, C. Sun, C. Yang, M. Xiao, L. Meng and Y. Li, *Nat. Commun.*, 2020, **11**, 2726.
13 B. Zhang, Y. Zhao, C. Xu, C. Feng, W. Li, X. Qin, M. Lv, X. Luo, X. Qin, A. Li, Z. He and E. Wang, *Adv. Funct. Mater.*, 2024, **34**, 2400903.
14 Z. Wang, N. Zheng, W. Zhang, H. Yan, Z. Xie, Y. Ma, F. Huang and Y. Cao, *Adv. Energy Mater.*, 2017, **7**, 1700232.
15 Z. Wang, H. Wang, M. Du, X. Lai, F. He, Q. Guo, Q. Guo, A. Tang, X. Sun and E. Zhou, *Adv. Funct. Mater.*, 2024, **34**, 2313240.
16 Z. Wang, H. Wang, L. Yang, M. Du, L. Gao, Q. Guo and E. Zhou, *Angew. Chem., Int. Ed.*, 2024, **63**, e202404921.
17 Z. Wang, X. Wang, L. Tu, H. Wang, M. Du, T. Dai, Q. Guo, Y. Shi and E. Zhou, *Angew. Chem., Int. Ed.*, 2024, **63**, e202319755.
18 D. Y. Kim, J. Subbiah, G. Sarasqueta, F. So, H. Ding, I. Irfan and Y. Gao, *Appl. Phys. Lett.*, 2009, **95**, 093304.
19 J. Subbiah, V. D. Mitchell, N. K. C. Hui, D. J. Jones and W. W. H. Wong, *Angew. Chem., Int. Ed.*, 2017, **56**, 8431–8434.
20 J. Subbiah, B. Purushothaman, M. Chen, T. Qin, M. Gao, D. Vak, F. H. Scholes, X. Chen, S. E. Watkins, G. J. Wilson, A. B. Holmes, W. W. H. Wong and D. J. Jones, *Adv. Mater.*, 2015, **27**, 702–705.
21 S. Chen, J. R. Manders, S.-W. Tsang and F. So, *J. Mater. Chem.*, 2012, **22**, 24202–24212.
22 Y. Zhou, C. Fuentes-Hernandez, J. Shim, J. Meyer, A. J. Giordano, H. Li, P. Winget, T. Papadopoulos, H. Cheun, J. Kim, M. Fenoll, A. Dindar, W. Haske, E. Najafabadi, T. M. Khan, H. Sojoudi, S. Barlow, S. Graham, J.-L. Brédas, S. R. Marder, A. Kahn and B. Kippelen, *Science*, 2012, **336**, 327–332.
23 L. Meng, Y. Zhang, X. Wan, C. Li, X. Zhang, Y. Wang, X. Ke, Z. Xiao, L. Ding, R. Xia, H.-L. Yip, Y. Cao and Y. Chen, *Science*, 2018, **361**, 1094–1098.
24 Z.-G. Zhang, B. Qi, Z. Jin, D. Chi, Z. Qi, Y. Li and J. Wang, *Energy Environ. Sci.*, 2014, **7**, 1966–1973.

25 C. Sun, Z. Wu, H.-L. Yip, H. Zhang, X.-F. Jiang, Q. Xue, Z. Hu, Z. Hu, Y. Shen, M. Wang, F. Huang and Y. Cao, *Adv. Energy Mater.*, 2016, **6**, 1501534.
26 J. Miao, Z. Hu, M. Liu, M. Umair Ali, O. Goto, W. Lu, T. Yang, Y. Liang and H. Meng, *Org. Electron.*, 2018, **52**, 200–205.
27 S. Shao, K. Zheng, T. Pullerits and F. Zhang, *ACS Appl. Mater. Interfaces*, 2013, **5**, 380–385.
28 M. Zi, X. Chen, S. Tan, C. Weng and B. Zhao, *Chem. Eng. J.*, 2022, **443**, 136455.
29 R. Samudrala, X. Zhang, R. M. Wadkins and D. L. Mattern, *Bioorg. Med. Chem.*, 2007, **15**, 186–193.
30 A. S. Jalilov, L. G. Nilewski, V. Berka, C. Zhang, A. A. Yakovenko, G. Wu, T. A. Kent, A.-L. Tsai and J. M. Tour, *ACS Nano*, 2017, **11**, 2024–2032.
31 A. K. Hundal, S. Ali, A. Agarwal, M. A. Jameel, L. A. Jones, J.-L. Li, R. A. Evans, S. J. Langford and A. Gupta, *J. Phys. Chem. Lett.*, 2021, **12**, 919–924.
32 P. Qin, T. Wu, Z. Wang, X. Zheng, X. Yu, G. Fang and G. Li, *Sol. RRL*, 2019, **3**, 1900134.
33 P. A. Finn, I. E. Jacobs, J. Armitage, R. Wu, B. D. Paulsen, M. Freeley, M. Palma, J. Rivnay, H. Sirringhaus and C. B. Nielsen, *J. Mater. Chem. C*, 2020, **8**, 16216–16223.
34 J. Subbiah, C. J. Lee, V. D. Mitchell and D. J. Jones, *ACS Appl. Mater. Interfaces*, 2021, **13**, 1086–1093.
35 H. Zhao, Y. Dou, S. Chen, H. Tang, Y. Bai, R. Tan, K. Zhang, C. Liu and F. Huang, *Chem. Mater.*, 2023, **35**, 8695–8705.
36 X. Du, T. Heumueller, W. Gruber, O. Almora, A. Classen, J. Qu, F. He, T. Unruh, N. Li and C. J. Brabec, *Adv. Mater.*, 2020, **32**, 1908305.